# CFD modelling approaches against single wind turbine wake measurements using RANS

**N Stergiannis[1,2,3,4], C Lacor[1], J V Beeck[2] and R Donnelly[3]**

[1] Vrije Universiteit Brussel, Department of Mechanical Engineering, Fluid Dynamics and Thermodynamics Research Group, Pleinlaan 2, 1050, Brussels, Belgium
[2] Von Karman Institute for Fluid Dynamics, Department of Environmental and Applied Fluid Dynamics, Waterloosesteenweg 72, 1640, Brussels, Belgium
[3] 3E S.A., Kalkkaai 6 Quai la Chaux, 1000 Brussels, 1000, Brussels, Belgium

E-mail: nikolaos.stergiannis@vub.ac.be, nstergiannis@gmail.com

**Abstract.** Numerical simulations of two wind turbine generators including the exact geometry of their blades and hub are compared against a simplified actuator disk model (ADM). The wake expansion of the upstream rotor is investigated and compared with measurements. Computational Fluid Dynamics (CFD) simulations have been performed using the open-source platform OpenFOAM [1]. The multiple reference frame (MRF) approach was used to model the inner rotating reference frames in a stationary computational mesh and outer reference frame for the full wind turbine rotor simulations. The standard $k-\varepsilon$ and $k-\omega$ turbulence closure schemes have been used to solve the steady state, three dimensional Reynolds Averaged Navier-Stokes (RANS) equations. Results of near and far wake regions are compared with wind tunnel measurements along three horizontal lines downstream. The ADM under-predicted the velocity deficit at the wake for both turbulence models. Full wind turbine rotor simulations showed good agreement against the experimental data at the near wake, amplifying the differences between the simplified models.

## 1. Introduction

During the lifetime of a wind farm, operating wind turbines will have to deal with wake effects and their interaction. Part of the wind power is extracted from their rotors and as a result a velocity deficit with increased levels of turbulence is developing downstream.

The so called wake effects are of great importance in wind farms since they can cause total power losses up to 30% [2–4]. The clustered wind turbines that are in a row will be affected from the upstream flow of a wake, causing power losses and unexpected loads from the turbulence fluctuations . To optimize the wind farms and reach the maximum potential production of installed wind turbines within a limited sized area, we have to understand the physics involved at the process and be able to predict in advance the wake expansion. In addition, early estimation of the wake characteristics can optimize the wind farm layout and so the downstream wind turbines can work in better conditions reducing the number of failures and as a sequence the OPEX.

Several linear mathematical models have been developed in order to predict such flows. Yet, all the models include assumptions and simplifications following experimental observations.

[4] Corresponding author. Tel:+32 484.55.28.10

Computational Fluid Dynamics (CFD), instead, provide more sophisticated methods, such as the Reynolds Averaged Navier-Stokes (RANS) equations, that can resolve the wind flow more accurately [5]. Following the trend of technological growth, the computational cost will continue to decrease on the years to come. Hence, the usage of CFD will be economically affordable for optimizing industrial applications. Over the last decades the CFD scientific community is growing and so on the ongoing research on turbulence modeling, numerical schemes, numerical methods and models, time and spatial filtering of fluid dynamics equations.

CFD simulations can be performed on both steady and unsteady state problems. It is common and acceptable, within limitations, the assumption of using a steady state approach to resolve a time-varying (unsteady state) problem when someone is interesting in the mean values of the flow that are statistically averaged in time. The RANS equations using two-equation models [6, 7] is a common approach with reasonable computational cost for applications involving flows of high Reynolds numbers. Other existing advanced methods, that are inherently unsteady, such as Detached Eddy Simulation (DES), Large Eddy Simulation (LES) and Direct Numerical Simulation (DNS) can be more accurate but the high computational cost makes them unattractive or even impossible today for use in industrial applications.

## 2. Mathematical model

### *2.1. Statement of the problem*

The physical problem under investigation is the flow over two identical wind turbines in a row under controlled conditions of a wind tunnel. The current study is focusing on the wake expansion and prediction by different CFD approaches.

### *2.2. Governing equations*

The governing equations solved of the flow field are the continuity and conservation of momentum equations:

$$\frac{\partial \rho}{\partial t} + \nabla \cdot (\rho \vec{u}) = 0 \tag{1}$$

$$\frac{\partial (\rho \vec{u})}{\partial t} + u \cdot \nabla (\rho \vec{u}) = -\nabla p + \nabla \cdot \tau + S_M \tag{2}$$

Where $\rho$ is the air density, $\vec{u}$ is the fluid velocity vector, $p$ the pressure, $\tau$ the shear stress tensor and $S_M$ a momentum source term. The stress tensor, is related to the strain rate as:

$$\tau = \mu \left[ \nabla \vec{u} + (\nabla \vec{u})^{\tau} - \frac{2}{3} \cdot \delta \cdot \nabla \vec{u} \right] = 0 \tag{3}$$

where $\delta$ is Kronecker's delta and $\mu$ is the dynamic viscosity of the fluid.

### *2.3. The Multiple Reference Frame (MRF) formulation*

The multiple reference frame (MRF) approach was used to model the internal rotating frames in a stationary computational mesh and reference frame.

The absolute velocity at the inertial reference frame, using the notation $i$ for inertial and $r$ for rotating, can be expressed as:

$$\vec{u}_i = \vec{u}_r + \vec{\Omega} \times \vec{r} \tag{4}$$

The acceleration is expressed as:

$$\left[ \frac{d\vec{u}_i}{dt} \right]_{inertial} = \left[ \frac{d\vec{u}_i}{dt} \right]_{rotating} + \vec{\Omega} \times \vec{u}_i \tag{5}$$

and by using the Eq.(4):

$$\left[\frac{d\vec{u}_i}{dt}\right]_{inertial} = \left[\frac{d\vec{u}_r}{dt}\right]_{rotating} + \frac{d\vec{\Omega}}{dt} \times \vec{r} + 2\vec{\Omega} \times \vec{u}_r + \vec{\Omega} \times \vec{\Omega} \times \vec{r} \tag{6}$$

Following the same notation, the incompressible RANS equations at the rotating frame of reference can be written in terms of absolute velocity at the inertial frame of reference:

$$\nabla \cdot \vec{u}_i = 0 \tag{7}$$

$$\nabla \cdot (\vec{u}_i \otimes \vec{u}_i) = -\nabla\left(\frac{p}{\rho}\right) + \nu\nabla \cdot \nabla(\vec{u}_i) \tag{8}$$

and at the rotating frame of reference:

$$\nabla \cdot \vec{u}_i = 0 \tag{9}$$

$$\nabla \cdot (\vec{u}_r \otimes \vec{u}_i) + \vec{\Omega} \times \vec{u}_r = -\nabla\left(\frac{p}{\rho}\right) + \nu\nabla \cdot \nabla(\vec{u}_i) \tag{10}$$

*2.4. Turbulence modeling*

Two-equation turbulence models are widely tested over the years and have been proved as an accepted compromise between accuracy and computational cost. At the current work the performance of several two-equation turbulence models on wake expansion was tested and compared with measurements. Those linear eddy viscosity models are using the Boussinesq assumption (Equation 11) for the Reynolds stresses:

$$\tau_{ij} = 2\mu_t\left(S_{ij} - \frac{1}{3}\frac{\partial u_k}{\partial x_k}\delta_{ij}\right) - \frac{2}{3}\rho k\delta_{ij} \tag{11}$$

where

$$S_{ij} = \frac{1}{2}\left(\frac{\partial u_i}{\partial x_j} + \frac{\partial u_j}{\partial x_i}\right) \tag{12}$$

- *$k-\varepsilon$ turbulence model*

The standard $k-\varepsilon$ model [9] is based on model transport equations for the turbulence kinetic energy, $k$ and its dissipation rate, $\varepsilon$. The model uses the following transport equations:

$$\frac{Dk}{Dt} = \frac{1}{\rho}\frac{\partial}{\partial x_k}\left[\frac{\mu_t}{\sigma_k}\frac{\partial k}{\partial x_k}\right] + \frac{\mu_t}{\rho}\left(\frac{\partial U_i}{\partial x_k} + \frac{\partial U_k}{\partial x_i}\right)\frac{\partial U_i}{\partial x_k} - \varepsilon \tag{13}$$

$$\frac{D\varepsilon}{Dt} = \frac{1}{\rho}\frac{\partial}{\partial x_k}\left[\frac{\mu_t}{\sigma_\varepsilon}\frac{\partial \varepsilon}{\partial x_k}\right] + \frac{C_1\mu_t}{\rho}\frac{\varepsilon}{k}\left(\frac{\partial U_i}{\partial x_k} + \frac{\partial U_k}{\partial x_i}\right)\frac{\partial U_i}{\partial x_k} - C_2\frac{\varepsilon^2}{k} \tag{14}$$

The turbulent viscosity $\mu_t$ is calculated from equation 15 below:

$$\mu_t = \rho C_\mu \frac{k^2}{\varepsilon} \tag{15}$$

According to the recommendations of Launder et al [10] the standard constants of the $k-\varepsilon$ model are given in Table 1.

**Table 1.** Constants of $k-\varepsilon$ turbulence model

| $C_\mu$ | $C_1$ | $C_2$ | $\sigma_k$ | $\sigma_\varepsilon$ |
|---|---|---|---|---|
| 0.09 | 1.44 | 1.92 | 1.0 | 1.3 |

- *$k-\omega$ turbulence model*

The basic transport equations for this two-equation model [7, 11] are:

$$\frac{Dk}{Dt} = P - \beta^* \rho\omega k + \frac{\partial}{\partial x_j}\left[\left(\mu + \sigma_k \frac{\rho k}{\omega}\right)\frac{\partial k}{\partial x_j}\right] \tag{16}$$

$$\frac{D\omega}{Dt} = \frac{\gamma\omega}{k} P - \beta\rho\omega^2 + \frac{\partial}{\partial x_j}\left[\left(\mu + \sigma_\omega \frac{\rho k}{\omega}\right)\frac{\partial \omega}{\partial x_j}\right] \tag{17}$$

where

$$P = \tau_{ij}\frac{\partial u_i}{\partial x_j} \tag{18}$$

and $\tau_{ij}$ derived from Equations 11 and 12.
The turbulent viscosity $\mu_t$ is computed from the following expression:

$$\mu_t = \frac{\rho k}{\omega} \tag{19}$$

The default model constants for the $k-\omega$ turbulence model are given in Table 2.

**Table 2.** Constants of $k-\omega$ turbulence model

| $C_\mu$ | $\sigma_k$ | $\sigma_\omega$ | $\beta^*$ | $\beta$ | $\gamma$ |
|---|---|---|---|---|---|
| 0.09 | 0.5 | 0.5 | 0.09 | 0.072 | 0.52 |

The $\gamma$ coefficient was chosen in order to yield an appropriate value for the von Karman constant ($\kappa \approx 0.41$), via the expression 20:

$$\gamma = \frac{\beta}{\beta^*} - \frac{\sigma_\omega \kappa^2}{\sqrt{\beta^*}} \tag{20}$$

*2.5. Wind turbine modeling*
For the case of actuator disk model, wind turbine rotors are approximated as momentum sinks to represent the axial thrust force $T$, associated with a constant uniform thrust coefficient $C_T$ over the rotor area:

$$T = 0.5\rho A C_T U_{ref}^2 \tag{21}$$

where $A$ is the surface area of the rotor-disk, $\rho$ the air density, $U_{ref}$ the undisturbed (from the rotor under investigation) reference free-stream velocity and $C_T$ the thrust coefficient of the rotor.

Once the $U_{ref}$ is known, the $C_T$ can be estimated through the thrust curve of the wind turbine generator considered as uniform over the rotor area [2]. However, in operating conditions, the flow across the rotor is very complex with varying span-wise properties mainly because of the blade characteristics, rotational velocity, turbulence, finite number of blades but as well as other flow characteristics related to non-uniform inflow conditions, atmospheric boundary layer shear and so on.

To overcome the limitations of the standard actuator disk model, several more advanced models like the generalized actuator disk, actuator line model, actuator surface, have been proposed [15].

The drawback of the advanced models is mainly that they need several input variables such as airfoil data, detailed blade geometry which most of the times are not available or confidential for industrial applications. Finally, most of the advance models require time resolved CFD simulations which increase the final computational cost [16].

The standard actuator disk model that was used in this study is implemented in OpenFOAM based on the induction factor $\alpha$:

$$\alpha = 1 - \frac{C_P}{C_T} \tag{22}$$

where $C_P$ the pressure coefficient.

The thrust force is then given by Equation 23:

$$T = 2\rho A\alpha(1-\alpha)U_{ref}^2 \tag{23}$$

In all the cases under investigation a constant uniform reference wind speed of $11.5\,m/s$ have been used. The coefficients $C_P$ and $C_T$ have been provided from the wind tunnel measurements and were used as inputs to the simplified models for a straightforward comparison of their performance at the wake expansion.

## 3. The 4th blind test experiment

The 4th Blind Test (BT4) experiment was organized by NOWITECH and NORCOWE in 2015. The total power output from two in-line turbines was investigated under the influence of different inlet conditions and turbine separation distance. [8].

The axial separation distance between the turbines was set to $x/D = 2.77$, $x/D = 5.18$ and $x/D = 9.00$, where the diameter $D = 0.894m$. Furthermore, three different inflow conditions at the inlet of the test section were tested:

- Low turbulence uniform inflow: No grid at the inlet to the test section. At the position of the upstream turbine the turbulence intensity measured is $TI = 0.23\,\%$. The mean wind speed is uniform across the test section, apart from small wall boundary layer effects.
- High turbulence uniform inflow: An evenly spaced turbulence gird at the tunnel inlet generates a higher turbulence intensity level of $TI = 10.0\,\%$ at the location of the upstream turbine. The mean wind speed is uniform across the test section.
- High turbulence shear inflow: A turbulence grid with increasing vertical distance between the horizontal bars is installed at the inlet of the test section. This is creating a non-uniform shear flow with a mean turbulence intensity of $TI = 10\,\%$ over the rotor swept area of the upstream turbine.

The high Turbulence Intensity (TI) CASE-B was tested on three different downstream axial separation distances of $x/D = 2.77$, $x/D = 5.18$ and $x/D = 9$, where the diameter $D = 0.894\,m$.

In our study, CASE-B3 of high TI and $x/D = 9$ axial separation distance was chosen to eliminate the impact of the second wind turbine at the single wake expansion of the first and because more measured data were available downstream. A uniform velocity profile of $11.5\,m/s$ similar to the experiment for the CASE-B3 was considered. The two wind turbines are constructed with the same aluminum blades, using the NREL S826 airfoil section from root to tip.

## 4. Full rotor CFD simulations

To address the question of how much information is lost with the simplified models, results are compared with more advanced CFD simulations that include the full wind turbine rotor geometries and their hubs.

### *4.1. Computational domain*

The computational domains were designed to match the exact wind tunnel dimensions to represent the experimental setup and account for possible blockage effects (Fig. 1). Particularly for the CASE-B3, the domain have been extended by $3.7\,m$ in length (30 % of total) to avoid any numerical oscillations from the outlet at the far wake measurements downstream.

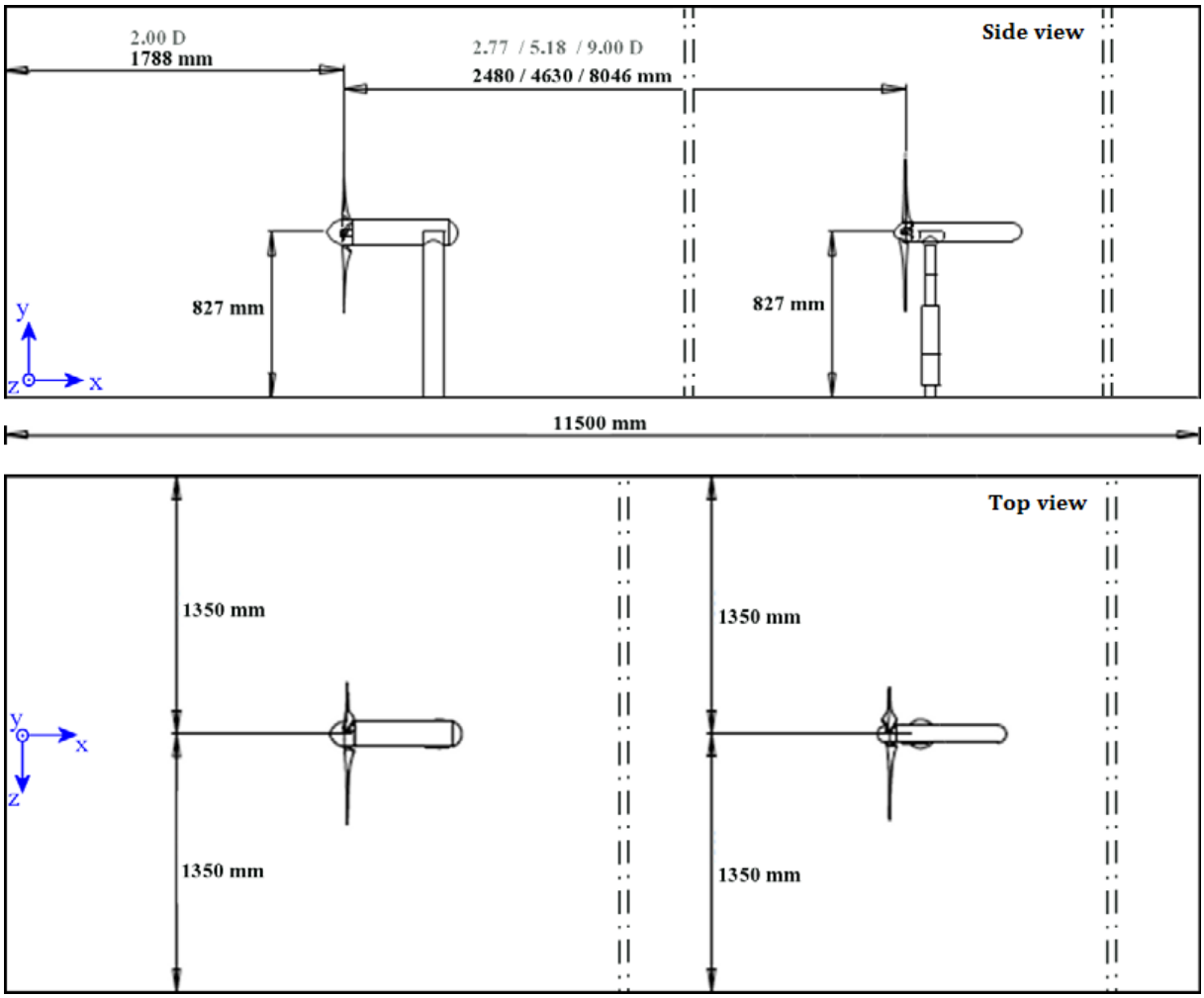


**Figure 1.** Wind tunnel dimensions and wind turbine positioning at the reference coordinate system.

The *blockMesh* utility of OpenFOAM platform with in-house code was used to generate a multi-block hexahedral computational mesh of $670k$ cells. That mesh was further modified and refined in regions of interest with the more advanced *snappyHexMesh* utility. Different refinements have been tested at the rotor-wake region with actuator disk rotors and the $k-\varepsilon$ turbulence model to achieve a mesh independent solution. The hexahedral mesh elements of the background mesh (M1 = 0.67Mi cells) were doubled at each coordinate on every new level of refinement. Three meshes M2, M3, M4, of 2.91Mi, 11.9Mi and 92.6Mi cells respectively, have been generated using three different levels of refinement. Steady state solutions using RANS and second order schemes, converged with residuals below $10^{-4}$. The axial velocity over the line L1 = $2.77D$ was compared and presented in Fig. 2. The difference between the M3 (fine) and M4 (very fine) computational meshes at the maximum velocity deficit of the single wake (minimum axial velocity at the rotor center) over line L1 was $0.025m/s$. The M3 (fine) mesh, proved to be a good compromise of accuracy and computational cost and was chosen for all the CFD simulations.

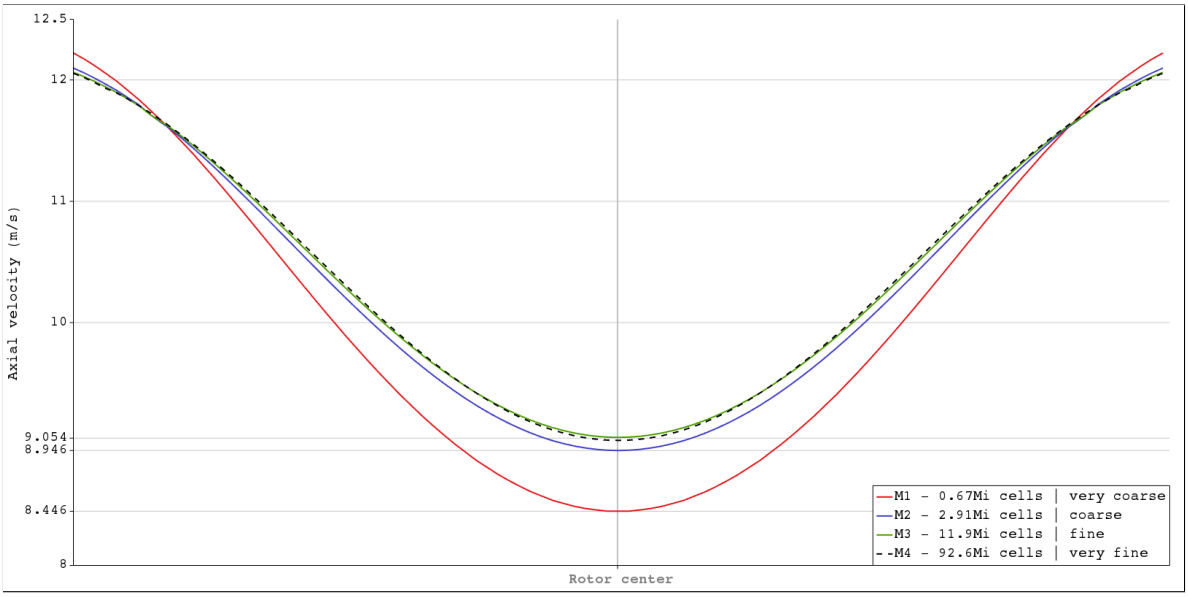


**Figure 2.** Mesh independence test using actuator disk models and the $k-\varepsilon$ turbulence model. Plots of the axial velocity at the hub height and over line L1 = $2.77D$ downstream of the first wind turbine rotor.

For the full rotor cases, before the snapping of the mesh at the imported surfaces several local refinements have been done at the blades (level 6) and the hubs (level 5) of the wind turbines, using four transitional cells between the refinement levels. (Fig. 3, BOTTOM-LEFT). Four cell-layers were also added normal to the surfaces of the geometries with an expansion ratio of 1.5 (Fig. 3, BOTTOM-RIGHT). The global cell size at the centered block of the mesh was $0.0675^3\,m^3$. According to each refinement level, those cells have been refined down to $0.016875^3\,m^3$ (level 1) and $0.003375^3\,m^3$ (level 2), whereas the cells close to the geometries had a global size of $0.00105^3\,m^3$ (level 5) and $0.0007^3\,m^3$ (level 6) at the surface. The final fine computational mesh size was 30Mi cells for the full rotor CFD simulations and 14Mi cells for the ADM case.

At the design condition for a Tip Speed Ratio (TSR) $\lambda = \Omega R\,/\,U_{ref} = 6$, the Reynolds number at the tip is $Re_c = \lambda U c_{tip}\,/\,\nu \approx 10^5$. Therefore the above cell sizes ensure that high-Reynolds wall functions can be applied at the first cell to the walls.

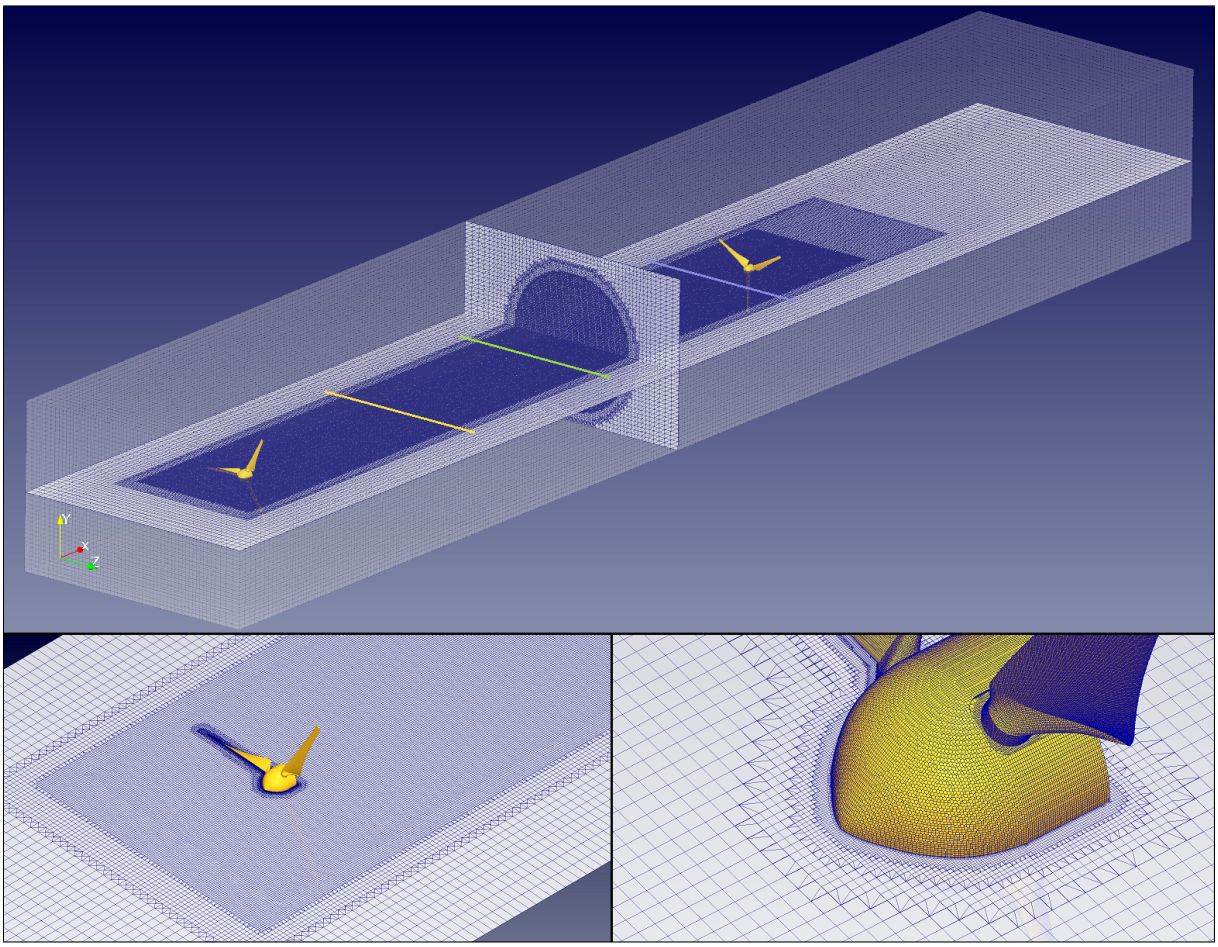

**Figure 3.** The fine mesh (M3) that was used for the CFD simulations. Top: details of the multi-block mesh and refinements that were generated with *blockMesh* and *snappyHexMesh* utilities. The three horizontal lines represent the measurements at the hub height $h_{hub} = 0.827m$ over the L1 (yellow) $= 2.77D$, L2 (green) $= 5.18D$ and L3 (blue) $= 8.5D$ lines downstream of the first rotor. BOTTOM-LEFT: rotor-wake region using a refinement of level 2. BOTTOM-RIGHT: surface cells and surface layers close to the geometry.

*4.2. Solution methodology and boundary conditions*

All the simulations have been performed in the open-source CFD platform OpenFOAM, using the steady state incompressible solver *simpleFoam* which is based on the Semi-Implicit Method for Pressure-Linked Equations (SIMPLE) algorithm.

Initial values and inlet values for the turbulence characteristics were estimated by using the experimental measured $TI$ and the turbulent length scales $\ell$ of each case with the following expressions:

$$k = \frac{3}{2}\left(\overline{U}TI\right)^2 \tag{24}$$

$$\varepsilon = C_\mu^{0.75}\frac{k^{1.5}}{\ell} \tag{25}$$

$$\omega = C_\mu^{0.75}\frac{\sqrt{k}}{\ell} \tag{26}$$

where $\overline{U} = U_{ref} = 11.5\,m/s$ and density of air $\rho = 1.25\,kg/m^3$.

The boundary conditions that were used are summarized in Tables 3 and 4.

**Table 3.** Inflow and outflow boundary conditions

| | Dirchlet Fixed value | Neumann Zero gradient |
|---|---|---|
| Inlet | $\vec{U}$, $k$, $\varepsilon$, $\omega$ | $p$ |
| Outlet | $p = 0$ | $\vec{U}$, $k$, $\varepsilon$, $\omega$ |

**Table 4.** Other boundary conditions

| | |
|---|---|
| Sides, top and bottom | Slip condition |
| Blades, hubs, nacelles, towers | Wall functions |
| Actuator Discs | Momentum sinks |
| Rotating Frame WT1 | TSR: $\lambda = 6$ |
| Rotating Frame WT2 | TSR: $\lambda = 4 - 5$ |

## 5. Results and discussion

For the cases under investigation, qualitative and quantitative results of the wake expansion are given below. Two CFD modelling approaches have been tested using the standard two equation $k-\varepsilon$ and $k-\omega$ turbulence models. Results showed different wake expansion for both approaches and for each turbulence model (Figures 4, 5).

### *5.1. Predictions of the axial velocity and turbulence kinetic energy (TKE) contours*

The differences between the simplified ADM and the full rotor CFD simulations can be observed qualitative by comparing the contours of the velocity and turbulence kinetic energy at xz-plane at hub height ($h_{hub} = 0.827m$).

For the simplified case of the standard actuator disk model, the wake recovery occurs in a shorter distance compared to the full rotor CFD simulations (Fig. 4, TOP). This could be

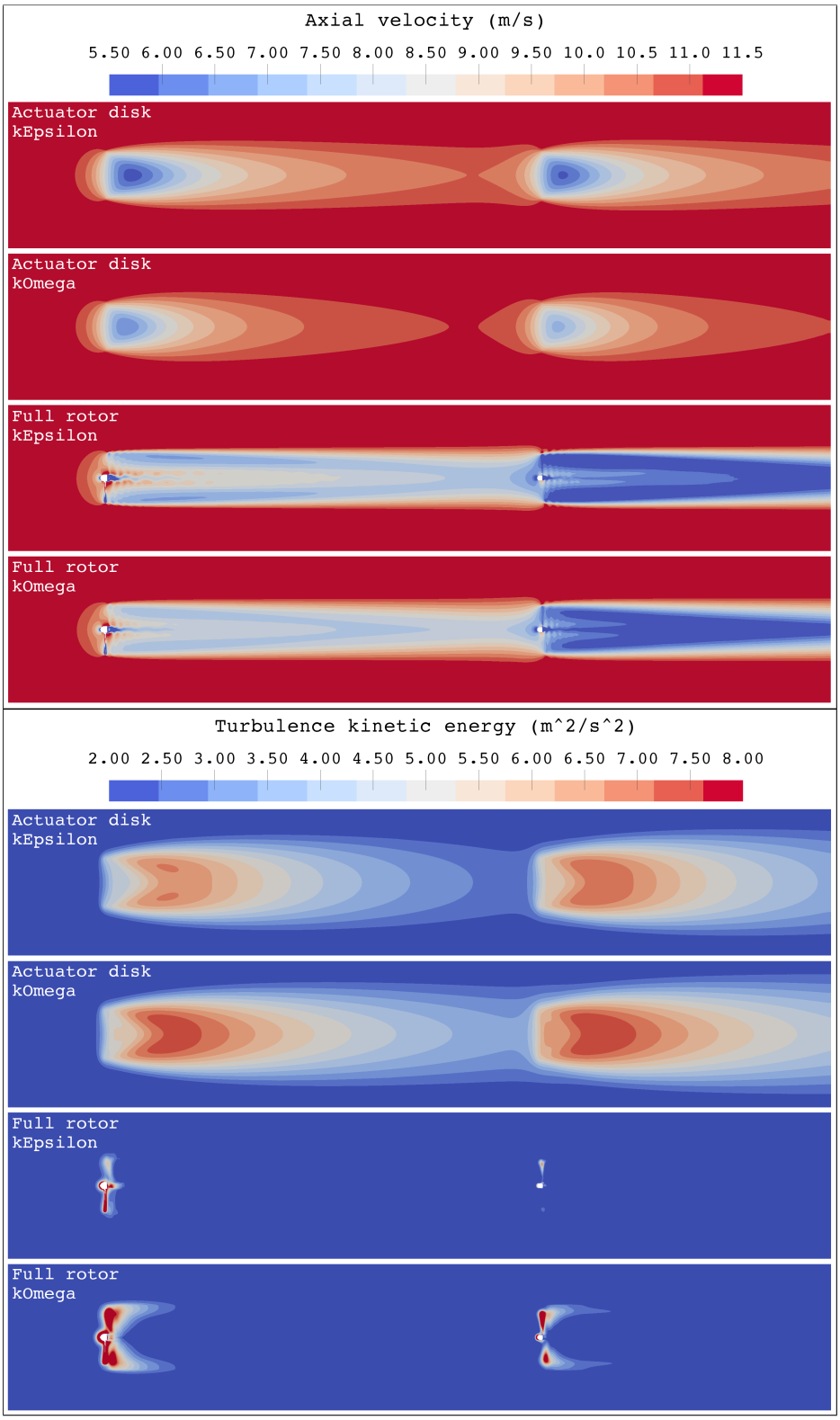


**Figure 4.** Horizontal xz-planes at $h_{hub}$.

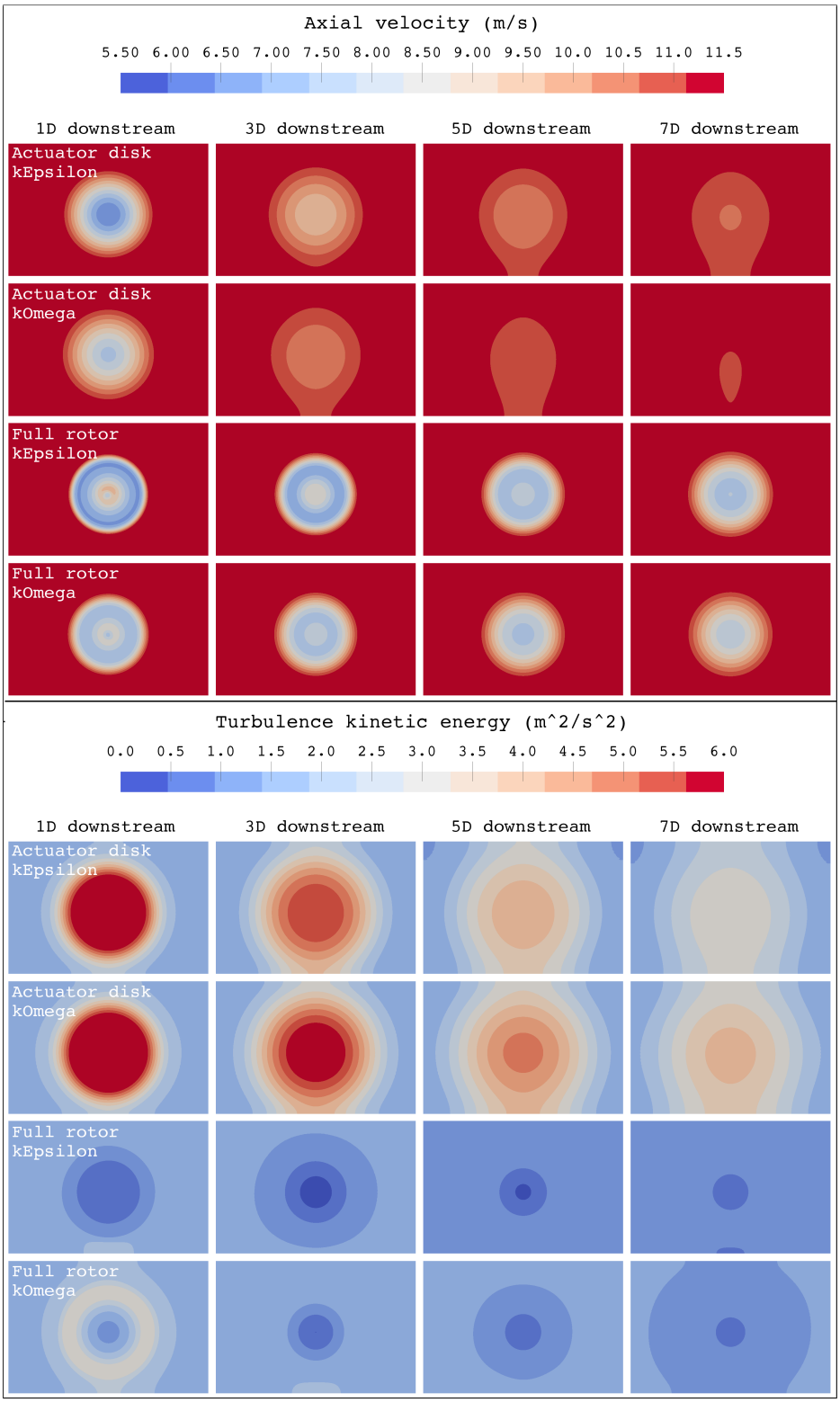


**Figure 5.** Vertical yz-planes at several positions downstream of the first wind turbine.

related to the enhanced turbulence production at the wake region observed in Fig. 4, BOTTOM. Further details of the wake development downstream can be observed at the vertical planes of axial velocity and TKE downstream of the first wind turbine rotor (Fig. 5).

*5.2. Comparison against measurements*

Wake profiles along three horizontal lines behind the upstream wind turbine rotor and at the elevation of the center of the turbine hub ($h_{hub}$) were extracted covering an horizontal span width from $z = -944mm$ to $z = +944mm$. The three horizontal lines L1, L2, L3 are located $2.77D$, $5.18D$ and $8.5D$ downstream the first wind turbine rotor respectively. Calculated values of the normalized velocity $U^* = U_{wake}/U_{ref}$ are compared against the BT4 experimental data (Figures 7, 8).

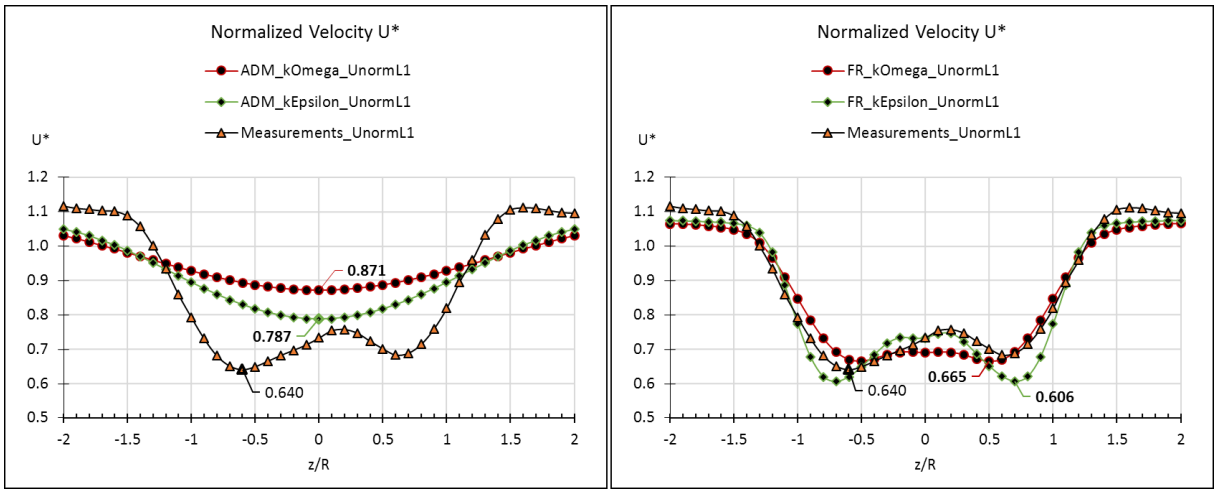


**Figure 6.** Normalized velocity against measurements over line L1 at $h_{hub}$. Comparison of $k-\varepsilon$ and $k-\omega$ turbulence models. LEFT: ADM. RIGHT: full wind turbine rotors.

A symmetrical U-shaped velocity profile is expected at the wake region and over horizontal lines at the disk center (hub height) when a uniform momentum sink of constant thrust is applied [2]. The plots of normalized velocity (Fig. 7) verify that behavior for both turbulence models. In addition, the presence of the actuator disks in the flow field causes shearing at their circumferences, resulting to generation of turbulence ("double peak" values) which is also captured at the contours of the turbulence kinetic energy (Fig. 4, BOTTOM).

ADM underestimated the velocity deficit at all the wake regions downstream with both turbulence models. At the near wake, line L1, a difference of 10.67% is observed between the predictions of the two models. The $k-\varepsilon$ predicted a minimum normalized velocity $U^* = 0.787$ whereas the $k-\omega$ a minimum $U^* = 0.787$. The minimum measured value over line L1 was $U^* = 0.640$. The difference of the minimum normalized velocities between predictions and measurements were 22.97%, 36.09% for the $k-\varepsilon$ and $k-\omega$ turbulence models respectively. Plots of normalized velocities for both turbulence models against measurements over the line L1 at $h_{hub}$ are given in Fig. 6. Further downstream at the far wake, ADM predictions had a difference of 26.83%, 34.86% over line L2 and 12.71%, 17.84% over line L3, for the $k-\varepsilon$ and $k-\omega$ turbulence models respectively (Fig. 7).

The full wind turbine rotor simulations predicted more accurately the near wake, capturing also the shape of the velocity deficit (Fig. 6). Using the $k-\varepsilon$ turbulence model, predictions against measurements had a difference of 5.31%, 6.6% and 19.64% over lines L1, L2 and L3 respectively. The $k-\omega$ turbulence model performed better with the full wind turbine rotor

simulations, predicting minimum values of normalized velocities with a difference of 3.91%, 2.87% and 14.63% over lines L1, L2 and L3 against measurements (Fig. 8).

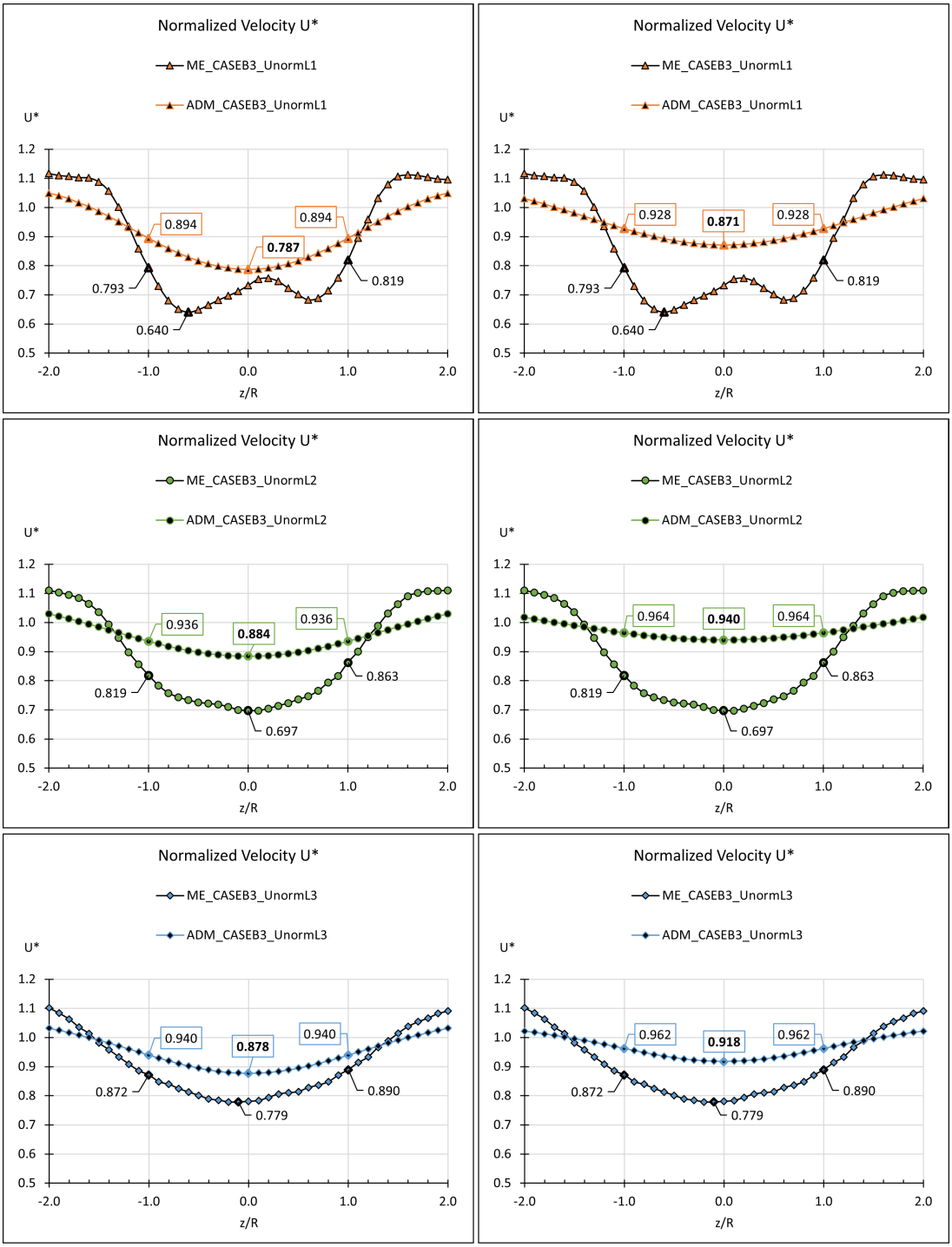


**Figure 7.** Results of actuator disk model simulations against measurements over three horizontal lines at the wake of the upstream wind turbine rotor. From TOP to BOTTOM: L1, L2 and L3. LEFT: $k-\varepsilon$ turbulence model. RIGHT: $k-\omega$ turbulence model.

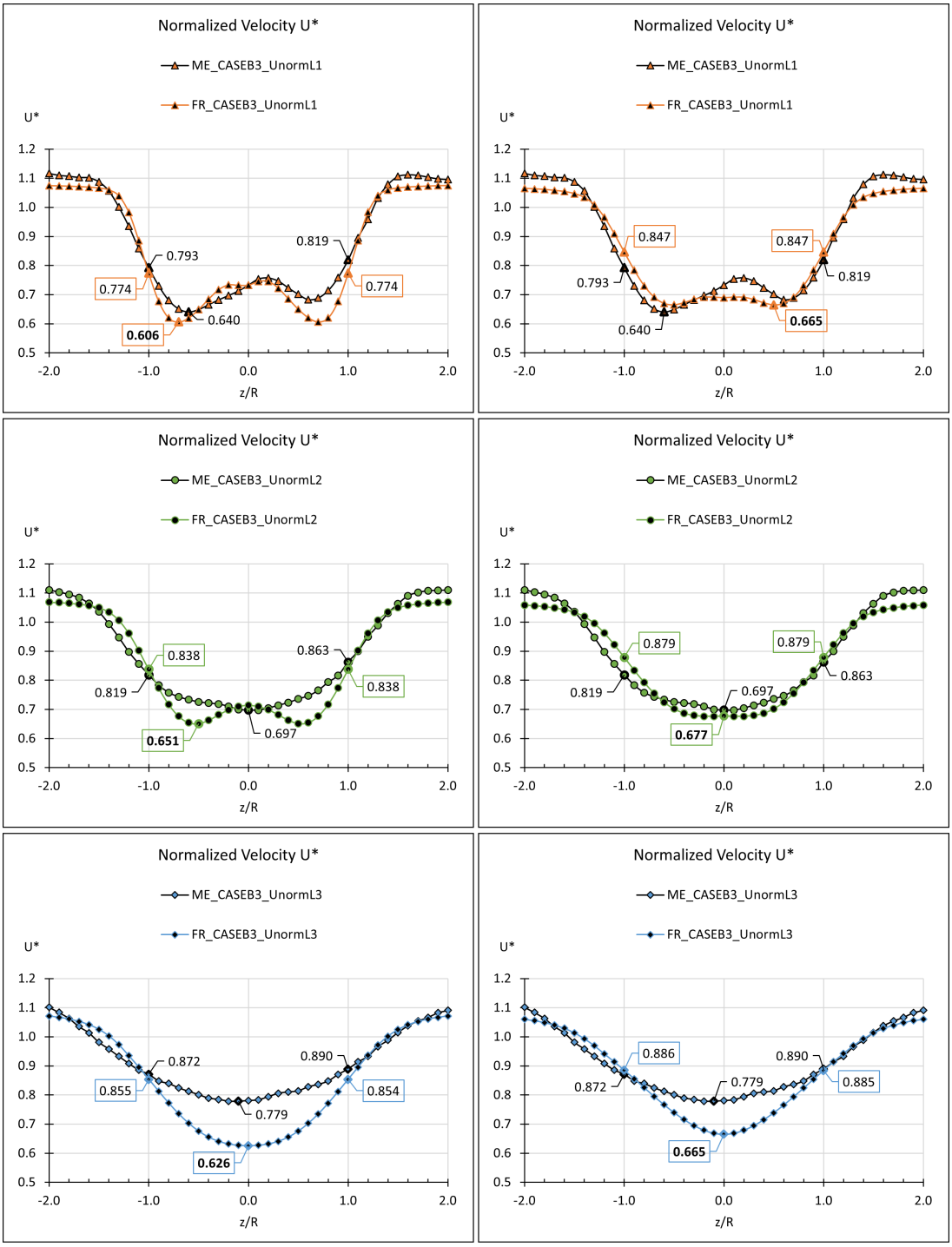


**Figure 8.** Results of full wind turbine rotor CFD simulations against measurements over three horizontal lines at the wake of the upstream wind turbine rotor. From TOP to BOTTOM: L1, L2 and L3. LEFT: $k-\varepsilon$ turbulence model. RIGHT: $k-\omega$ turbulence model.

The incapability of predicting the far wake downstream for the case of full wind turbine rotors can be related to the absence of the nacelles and towers. The presence of those components would

increase the TKE downstream forcing the velocity deficit to recover sooner and thus follow the trend that was observed in measurements.

## 6. Conclusions

The single wake expansion of an upstream wind turbine was investigated under controlled conditions of a wind tunnel, using different CFD modelling approaches. The OpenFOAM open-source platform was used, using the multiple reference frame (MRF) utility (for the case of the full wind turbine rotor) and the standard actuator disk model with the incompressible, steady state solver simpleFOAM.

Two numerical approaches have been tested on both $k-\varepsilon$ and $k-\omega$ turbulence models. The full rotor CFD simulations including the exact wind turbine geometries with their hubs and simulations with the implemented in OpenFOAM standard actuator disk model that represented the wind turbines in the flow field as momentum sinks. Comparison was made against experimental data at three downstream positions over horizontal lines at hub height.

The $k-\varepsilon$ turbulence model had a better agreement with the experimental measurements for the case of ADM, whereas for the full wind turbine rotors simulations the $k-\omega$ performed better. Results from the full wind turbine rotors simulation were in very good agreement with the measurements over the lines L1 and L2. For the far wake region and over the line L3 the predicted values over-estimated the velocity deficit. This behavior can be related to the absence of the nacelles and towers, since their presence is expected to increase the TKE and benefit the wake recovery.

In all cases, the ADM under-predicted the wake effects downstream, a behavior that was observed also by other studies [2, 3, 16, 20, 21]. Especially for the downstream distance of five diameters, which is of high interest since it is commonly used by industry as a separation distance in wind farms, results showed that there is a lack of capturing accurately the velocity deficit with the standard actuator disk model. Results of ADM, as it can be seen on Fig. 4, 5, are also very sensitive to the chosen turbulence model.

The present study address the question of how much information of the wake is lost when we move to a simplified model. Wind energy industry needs more advanced and accurate models to estimate better the wake losses and limit the risks of new potential wind projects as well as optimizing and operating more efficiently the existing ones. In line with the above, the research group of the authors are investigating a new actuator ring model, proposed by the author in 2013 [20], that will couple the advantages of a Blade Element Method (BEM) and actuator disk theory for steady state simulations. The model will aim to advance the employment of CFD simulations by the industry for wind energy applications.

## Acknowledgments

This work has been funded by INNOVIRIS, formerly known as the ISRIB (Institute for the encouragement of Scientific Research and Innovation in Brussels), the Brussels Institute for the promotion of scientific research and innovation, in the framework of the DOCTIRIS program and under the research project:

***"Non-deterministic advanced CFD modeling of wind turbine wakes and their interaction with applications to wind farms including complex terrain effects"***.

The authors acknowledge the Norwegian Technical National University (NTNU) for providing the experimental data of Blind Test 4 and professors Lars Roar Stran and Per-ge Krogstad for their support.

## References

[1] OpenFOAM 2016 openfoam.org URL `www.openfoam.org`
[2] Rados K, Mosfilis S, Stergiannis N, Tourlidakis A, Caralis G and Zervos A 2012 *European Wind Energy Conference and Exhibition 2012, EWEC 2012* vol 3 pp 1842–1849 ISBN 9781627482912
[3] Prospathopoulos J, Politis E, Rados K and Chaviaropoulos P 2011 *Wind Energy* **14** 285–300
[4] Barthelmie R J, Rathmann O, Frandsen S T, Hansen K S, Politis E, Prospathopoulos J, Rados K, Cabezón D, Schlez W, Phillips J, Neubert A, Schepers J G and van der Pijl S P 2007 *Journal of Physics: Conference Series* **75** 012049 ISSN 1742-6596
[5] Bazilevs Y, Hsu M, Kiendl J, Wüchner R and Bletzinger K 2011 *International Journal for Numerical Methods in Fluids* **65** 236–253
[6] Markatos N C 1986 *Applied Mathematical Modelling* **10** 190–220
[7] Wilcox D 1993 *Turbulence modeling for CFD* second edi ed vol 93 (DCW Industries) ISBN 0963605100
[8] Sætran L and Bartl J 2015 *Invitation to the 2015 "Blind test 4" Workshop Combined power output of two in-line turbines at different inflow conditions*
[9] Launder B E and Spalding D B 1974 *Computer Methods in Applied Mechanics and Engineering* **3** 269–289 ISSN 00457825
[10] Launder B E, Morse A, Rodi W and Spalding D B 1973 *NASA. Langley Res. Center Free Turbulent Shear Flows* vol 1 pp 361–426
[11] Wilcox D C 2008 *AIAA Journal* **46** 2823–2838 ISSN 0001-1452
[12] Menter F R 1994 *AIAA* **32** 1598–1605
[13] Menter F R, Kuntz M and Langtry R 2003 *Turbulence Heat and Mass Transfer 4* **4** 625–632
[14] Hellsten A 1998 *29th AIAA, Fluid Dynamics Conference* 1–11
[15] Mikkelsen R 2003 *Actuator disc methods applied to wind turbines* Ph.d thesis Technical University of Denmark
[16] Sanderse B, Pijl S and Koren B 2011 *Wind Energy* **14** 799–819 ISSN 10954244
[17] Bazilevs Y, Hsu M C, Akkerman I, Henicke B, Spielman T and E Tezduyar T 2011 *International Journal for Numerical Methods in Fluids* **65** 207–235
[18] Troldborg N, Sorensen J N and Mikkelsen R 2010 *Wind Energy* **13** 86–99 ISSN 10954244
[19] Vermeer L J, S"ø"rensen J N and Crespo A 2003 *Progress in Aerospace Sciences* **39** 467–510 ISSN 03760421
[20] Vafiadis K, Stergiannis N, Tourlidakis A and Rados K 2013 *European Wind Energy Conference and Exhibition, EWEC 2013* vol 3 pp 1692–1700 ISBN 9781632663146
[21] Crasto G, Gravdahl a R, Castellani F and Piccioni E 2012 *Energy Procedia* **24** 385–392 ISSN 18766102